Navigation and Localization via Wave Interference Patterns: An approach inspired by Marshallese Stick Charts

Leonardo Bobadilla[1], Dylan A. Shell[2], and Ryan N. Smith[3]

***Abstract*—Navigation and localization problems are challenging to solve when operating in ocean environments owing to inherent environmental dynamics and severe limitations on communication capabilities. This is compounded in coastal regions, precisely where the majority of the phenomena of interest occur, and the need for accurate navigation estimates is most critical. Existing navigation and localization techniques rely either on high-powered sensors (e.g., Doppler Velocity Loggers) resulting in decreased deployment time, or dead-reckoning (compass and IMU), with motion models resulting in poor navigational accuracy due to unbounded sensor drift combined with large environmental disturbances. Here we examine a low-cost, low-energy approach to navigation and localization in near-shore ($<100\,\mathrm{km}$) environments by considering non-metric instantiations of maps.**

Ocean navigation methods in the Marshall Islands up through the last century relied upon knowledge of charts made of sticks, shells, and engravings to aid seafarers in long sea voyages. These charts hold a wealth of information about the ocean in a seemingly simple representation of what we would call a map. In this paper, we examine the utility of a non-metric map representation that incorporates moving currents, wind directions, swell, and fluid-dynamic properties of refraction and reflection — data regarding the intrinsics of the ocean most germane where a geometric or absolute reference frame becomes less obviously the appropriate representation. We provide simulation results for both navigation and localization problems, and propose a simple control law for a practical navigation problem.

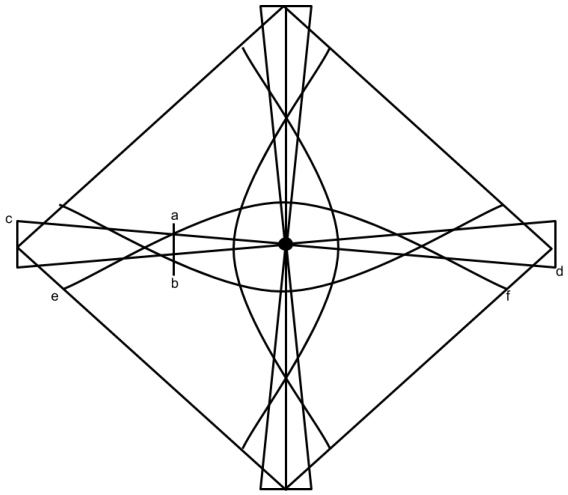

Fig. 1. A typical Marshallese *Mattang* stick chart used to help teach sailors how to conceptualize the wave patterns around islands [1]. Line *ab* represents the direction of the swell wave. The straight lines, e.g., line *cd*, divide the space around the island into quadrants, and the curved lines, such as line *ef*, represents the swell wave reflection off of the island.

I. Introduction

Modern oceanic navigation relies heavily on GPS. However, GPS requires connection to three satellites at minimum, the signal of which can be unreliable for a myriad of reasons: proximity to the north or south poles, attenuation from atmospheric conditions, sensor malfunction, or active blocking by human-caused RF interference. In pursuing the development of navigational methods that do not rely on GPS, we investigated the utility of historical forms of navigation coupled with today's technology.

Early ocean navigation methods in the Marshall Islands relied upon knowledge of charts made of sticks, shells, and engravings to aid seafarers in long sea voyages. These charts hold a wealth of information about the ocean in a seemingly simple representation. The representation contains information that we would associate to a map. Ocean navigation was treated via a heuristic, topological structure rather than a rigid, metric construct. Today, the concept of a map—as most often used in robotics—is a spatial abstraction to answer pairwise distance queries, the typical ends being route-finding and planning for autonomous navigation. However, when considering ocean navigation, it is obvious that navigation costs (and their variances) are no longer simple functions well-characterized by considerations of pure geometry, certainly not geometry fixed to an external reference frame. Traditional maps affix dynamic water-based phenomena to particular locations—we wish to reduce the 'tyranny of place' in its role as a unifying abstraction. We are interested in a synergy of Marshallese-like intuitions with metric maps to increase the autonomy of persistent and long-range assets in the maritime environment. Specifically, we are interested in combining representations that incorporate moving currents, wind directions, swell, and fluid-dynamic properties of refraction and reflection; the intrinsics of the ocean where a geometric or absolute reference frame becomes

[1] L. Bobadilla is with the School of Computing and Information Sciences, Florida International University, Miami, FL, USA. (e-mail: bobadilla@cs.fiu.edu)

[2] Dylan A. Shell is with the Department of Computer Science and Engineering, Texas A&M University, College Station, TX, USA. (e-mail: dshell@tamu.edu)

[3] Ryan N. Smith is with the Department of Physics and Engineering, Fort Lewis College, Durango, CO, USA. (e-mail: rnsmith@fortlewis.edu)

less obviously the appropriate representation. In this work, we explore how modern tools (compass, IMU, and simple control laws) can be used to perform accurate, persistent, long-distance navigation for autonomous maritime vehicles. Specifically, we use information from the wave spectrum to augment existing methods (dead-reckoning) to improve low-power navigation and localization.

II. Background

A. Stick Charts

Stick charts have been of interest to Western anthropologists since they were discovered by American missionary Gulick in 1862 [1], [2]. The stick charts served as an aid in teaching Marshallese sailors how to navigate using the wave patterns they experience while situated in a boat [3]. The combination of constructive and destructive interference between the reflections and refractions of waves among the Marshall Island chain provided a landmark-based roadmap for accurate navigation to distant islands within the region. The need for this type navigation in the Marshall islands was partly driven by the low height of the islands (lack of visual references/landmarks) and seasonal wind and wave patterns (consistent tradewinds and predictable dominant swell direction) [4]. Marshallese navigators used swell direction, current direction, wind direction and the direction of sunrise and sunset to aid in their navigation [5]. A *Vaeakau-Taumako*, or wind compass, was used to determine wind direction [6]. The direction of the wind, the sunrise and the sunset were used in tandem to give a sense of direction, similar in effect to a magnetic compass [5]. The swell and current directions were used to visualize the wave patterns [5].

There are three primary types of Marshallese stick charts; the *Mattang*, the *Meddo*, and the *Rebbelib* [7]. The *Mattang* (shown in Fig. 1) is an idealized chart, and the most widely referenced and utilized, without any sense of scale or distance. The primary purpose of this chart is to describe the way waves interact around a given island or archipelago [8]. To interpret the *Mattang*, shown in Fig. 1, imagine a single island at the center of the chart. The short stick (line *ab*) represents the direction of the incoming swell wave. This line *ab* is the only non-symmetric part of this kind of stick chart. The straight lines (e.g., *cd*) help to divide the region around the island into quadrants and the curved sticks, e.g., line *ef*, represents the waves reflected off of the island. The intersections between the curved sticks and straight sticks (e.g., line *cd*) are locations that a sailor should be able to sense based on the motion of a boat in the waves [1]. The sailor would use their ability to sense the motion of the waves to determine the direction of the island from up to 80 km away [9], [10].

The *Meddo* and *Rebbelib* charts contain information about wave patterns similar to the *Mattang*, but are generally specific to a particular region, or specialized for a given season. The *Meddo* generally focuses on a smaller region with seasonal wave patterns noted around islands. The *Rebbelib* is a regional *map* containing fewer details about wave patterns, but held more information about the spatial relationship between islands [1]; of the three types of charts, being more metric than topological.

B. Wave Mechanics

Marshallese navigation relies heavily on the mechanics of ocean waves. Ocean waves can be described by the 2D wave equation

$$\frac{\partial^2 u}{\partial t^2} = v^2\left(\frac{\partial^2 u}{\partial x^2} + \frac{\partial^2 u}{\partial y^2}\right). \tag{1}$$

Here, u is the potential energy of the wave, v is the group velocity of the wave, t is time, and x and y are two orthogonal directions in the plane of the water.

Solutions to (1) usually take the form of sines and cosines, and because the equation is a linear differential equation, superpositions of solutions are also solutions. Equation (2) is the general solution to (1), where A is the amplitude of the wave, C is an offset value, λ is the wavelength, and ω is the temporal angular frequency:

$$u(x,y,t) = A\sin\left(\frac{2\pi}{\lambda}(x+y) - \omega t\right) + C. \tag{2}$$

Variables A and C are both initial conditions, while λ and ω are wave properties that define the speed of the wave, see (3). These solutions to the 2D wave equation are subject to boundary conditions such as Snell's law, conservation of energy, and the conservation of momentum:

$$v = \frac{\omega\lambda}{2\pi}. \tag{3}$$

Snell's law, described by (4) and shown visually in Fig. 2, describes how waves bend due to a change in speed. This is relevant to water wave theory because, as the bathymetry of water becomes shallower, the speed of the wave group decreases. This decrease in speed causes the waves to bend and wrap around an island. Snell's law dictates that waves will always collide perpendicularly to the island in the ideal case. The fact that the water waves will always collide perpendicularly comes from taking the limit as v_2 goes to 0 in (4). As $v_2 \to 0$, θ_2 must also go to 0; this phenomenon is *refraction*.

$$\frac{v_1}{v_2} = \frac{sin(\theta_1)}{sin(\theta_2)} = \frac{\lambda_1}{\lambda_2}. \tag{4}$$

Equation (3) shows that wave speed is a function of both temporal frequency and wavelength. A decrease in speed implies either a decrease in temporal frequency or wavelength; however, a decrease in temporal frequency would imply waves would 'stack up' in time, because we do not see this phenomenon occur we can then conclude that a decrease in speed causes the wavelength to decrease (or we say they 'stack up' in space.)

Some of the waves slowed due to the shallow bathymetry will, inevitably, collide with the shore. In an idealized model, these collisions are assumed to be perfectly elastic meaning that the momentum and the energy of the wave remains constant. With these two constraints, the waves will reflect back, returning in the direction from which they struck the island. This type of reflection means that we can treat the island as a point source of waves. The assumption that the island looks and acts like a point source holds for large distances from the island; when not in visible sight range of the island.

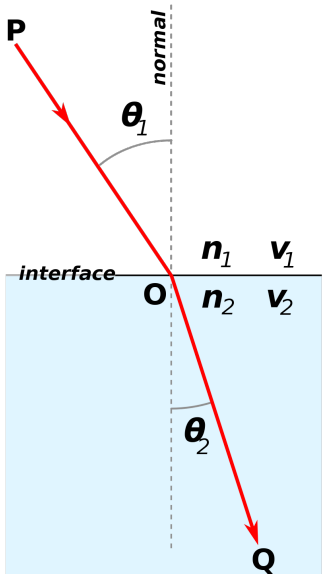

Fig. 2. Snell's law describes how incoming waves will bend owing to a change in speed. This change in speed occurs as the wave approaches shallower waters surrounding an island.

III. Computerized Simulation Model

For the purposes of testing modern technology to achieve navigation and localization based on historical Marshalese methods, we created a single-island, simulation environment. The island is treated as a point source, and the swell waves are treated as incoming planar waves. Reflections and refractions are then just superimposed to model the wave interaction around the island. Details of the simulated model appear in the sections which follow.

A. Creating the Simulation Environment

A computerized model was created to determine what parameters are necessary for accurate navigation and localization. The model was created in MATLAB using a relaxation differential equation solver. Equation (5) is the relaxation method used where u_n is the new potential, u is the current potential, u_p is the previous potential, i is the index in the x-direction and j is the index in the y-direction. As this method relies on the state of adjacent nodes, nodes at the edge cannot be evaluated. Thus, the boundary at $i = 1$ (left side of the model in Fig. 3) changes as a function of time based on a sinusoidal input. This sinusoidal input creates a perfectly planar wave that refracts and reflects off of an island placed at the center of the model domain. The remaining three edge boundaries are all held constant. The constant boundaries that are perpendicular to the wavefronts (top and bottom in Fig. 3) remove energy from the potential, u.

$$u_n(i,j) = 2u_n(i,j) - u_p(i,j) + \frac{1}{2}\Big(u(i+1,j) + u(i-1,j) - 4u(i,j) + u(i,j+1) + u(i,j-1)\Big) \quad (5)$$

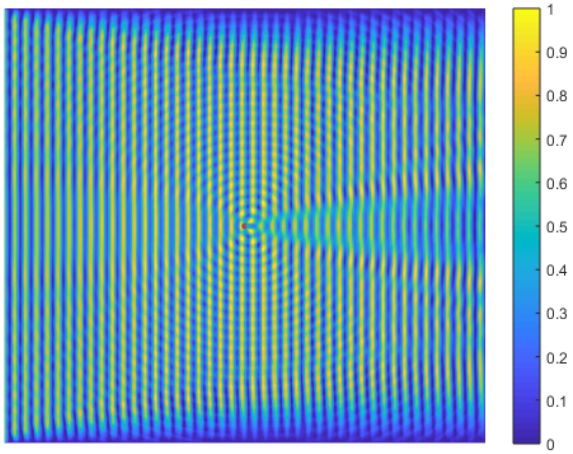

Fig. 3. Depiction of model at steady state where a swell wave is generated on the right hand side of the model, the swell wave is then refracted around the island and reflected. This figure shows the edge effects near the top and bottom of the model. The scale, on the right side of the figure, is relative potential energy, u, in the wave where 1 is the intensity of the incoming swell wave.

The steady state can be visualized in the snapshot in Fig. 3, where the shows wave potential, u, is rendered as a function of position, x across and y up, and time, t, or $f(x,y,t) = u$. The model space is 700×700 nodes in the x and y directions, with a temporal period of 16 time steps. Nodes with a distance less than ten nodes away from the island were changed to be less responsive to the states of adjacent nodes. This decrease in responsiveness in spatial coordinates slows the movement of the wave to model the refraction resulting from decreasing water depth. In this case, we have assumed that the bathymetry around the island decreases linearly. The change in speed around the island models how refraction occurs around islands due to changing bathymetry.

The top and bottom of the figure show drastic edge effects, owning to all the edges nodes having a fixed height of zero. (This boundary condition is a necessity of using a relaxation differential equation solver.) However, as these effects are confined to the edges of the model space, only the central nodes within $70 \leq x \leq 630$ and $70 \leq y \leq 630$ were examined.

B. Analyzing the Simulated Model

Two methods were used to examine the simulated environment: 1) numeric partial derivatives, and 2) Fourier transforms of the potential of the wave. These methods were performed spatially and temporally and were chosen partially due to their ease of measurement. Also, reports of the information that Marshallese sailors are said to sense suggest that frequency, amplitude, and associated energies are useful features. The potential energy of the wave is easy to measure because, when the depth of water is greater than the wavelength of the wave, the potential energy is directly proportional to the height of the wave.

Partial derivatives were found by connecting points on either side of the point of interest, and taking the slope of the

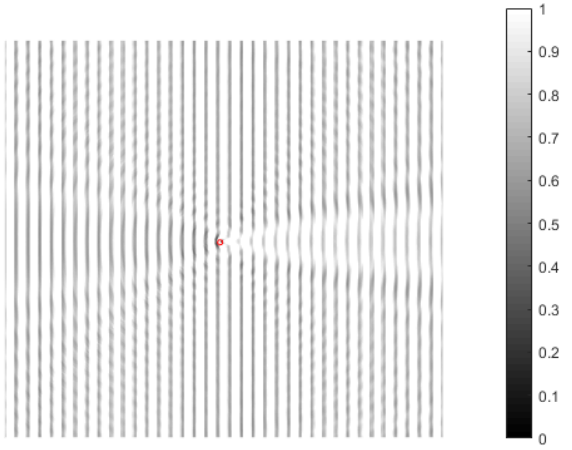

Fig. 4. Visualization of the partial derivative of the potential, u, in the x direction. The values of the partial derivative were then normalized between 0 and 1.

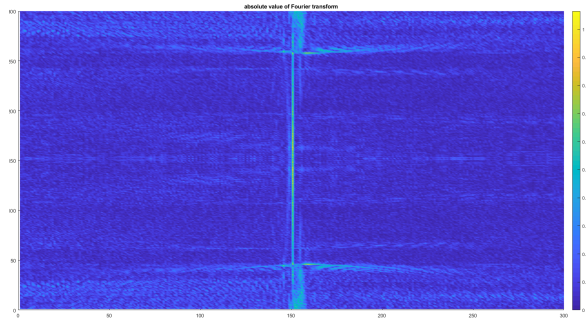

Fig. 5. Plot of the spatial Fourier transform, with a single high value at the center of the model when the swell wave crosses the island.

line (see. (6)). These first-order partial derivatives were taken with respect to x, y, and t. Figure 4 shows the value of the partial derivative in the x direction of the potential function u. The partials in the x and y directions were also represented as a gradient magnitude acting at an angle in the xy plane. The spatial partials represent how steep the wave is in a given direction, while the temporal partial gives how quickly the waves rise and fall at a specific point in space. These parameters describe the motion of waves that Marshallese navigators are said to have used/felt while navigating.

$$\frac{\partial f(x,y,t)}{\partial x} = \frac{f(x+1,y,t) - f(x-1,y,t)}{(x+1)-(x-1)} \tag{6}$$

Two types of Fourier transforms were performed on the model. The first was a spatial transform in both the x and y directions. This was done to see if there was any information encoded in the spatial frequency of the waves. The only information found with this transformation was at those particular times when the swell wave passes over the island (Fig. 5). The temporal Fourier transform was performed at each node of the model. Figure 6 shows that as distance to the island reduces, the temporal frequency increases. This increase in frequency is much higher when the distance is fewer than ten nodes.

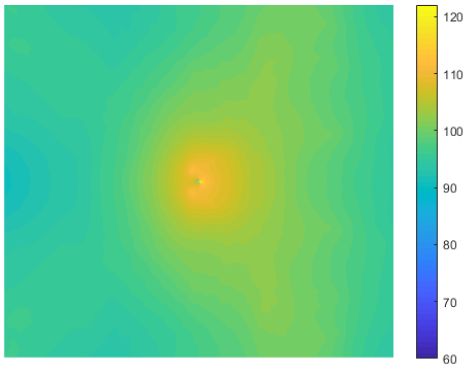

Fig. 6. Absolute value of the Fast Fourier Transform (FFT) of the potential u. The value of this FFT increases as one approaches the island. (The green dot in the middle of the figure is an artifact of how the island's node reflected waves.)

IV. Results

To navigate using wave patterns, one needs to be able to connect wave parameters and the location of the island. Here we employed supervised learning techniques to find such a relation. Supervised learning, as a form of machine learning, is used when the output is already known for a given data set. Given the computer model output, we have a collection of wave parameters at known locations relative to the island.

The two types of supervised learning are classification and regression. Classification takes a numeric input and gives a categorical output. The success of a classification machine is measured with accuracy, i.e., what percentage of outputs did the machine correctly label. While regression-type learning takes an numeric input and gives a numeric output, the success of which is measured with root mean squared error (RMSE), or the average distance between the output and the known value. Before supervised learning was used, the model space was split into four differing regions around the island (Fig. 7). This division into regions was done to mimic the symmetry observed in the *Mattang* chart (Fig. 1).

A. Navigation

The first application learning is a classification task: to determine which of the four regions a given observation occurred in. The inputs features provided were: potential as a function of time $u(t)$, potential gradient as a function of time $\frac{\partial u(t)}{\partial x}$ and $\frac{\partial u(t)}{\partial y}$, the time rate change of potential $\frac{\partial u(t)}{\partial t}$ and Fourier transform of potential FFT(u). A parametric study of different kernels was performed to see which would best correlate wave parameters to region. The kernel with the highest accuracy was a quadratic support vector machine (quadratic SVM), with an accuracy of 98.6%. To build the predictor, 15% of the available nodes (11.189 nodes per region) were selected from each region. A quadratic SVM machine learning kernel was then trained using five-fold cross validation with 15% of the

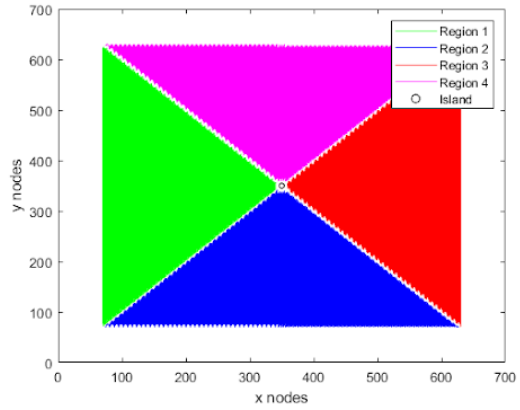

Fig. 7. For the purposes of learning, the spatial variables were divided into four equal-sized regions with the island at the center at point (350,350), and the 70 nodes around the edges removed to ignore the edge effects present in the model. A single line of nodes between each region was left unassigned and a total of 78323 nodes were in each region.

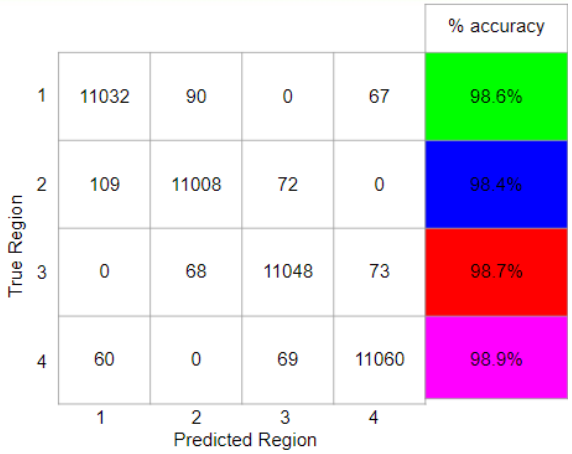

Fig. 8. Accuracy of the trained classifier: 15% of the available nodes (11.189 nodes per region) were selected from each region. A quadratic SVM machine learning kernel was then trained using five-fold cross validation with a 15% of the data held for validation.

data held out for final validation. Figure 8 shows the accuracy and error computed for each region.

The learned classifier was able to accurately determine which region around the island contained a given observation. An investigation of the errors indicates that they occurred specifically on the artificially inserted boundaries between the regions; areas where an observation could easily be in either of the two regions. This suggests that one could navigate to the island by associating each region to a direction to travel: a simple bang-bang controller. If in region one (green) go in the direction of the swell wave, if in region 2 (blue) turn left and go orthogonal to the swell wave, if in region 3 (red) go against the swell wave and if in region 4 (magenta) turn right and go orthogonal to the swell wave. In the event that an observation places you on a boundary, apply one of the

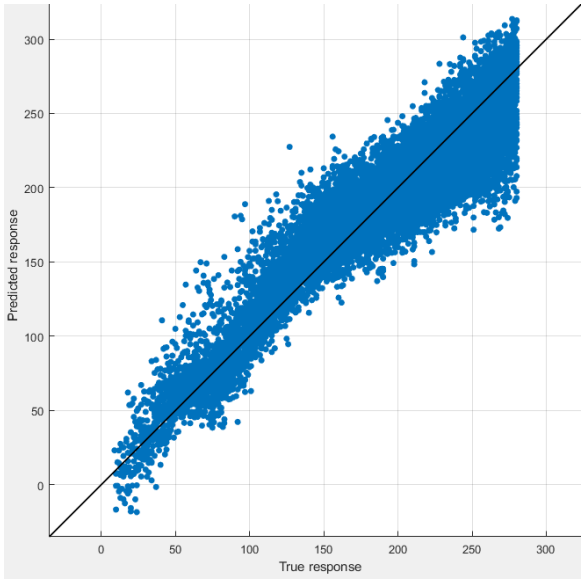

Fig. 9. True response versus predicted response for the regressor trained to determine the distance in the x direction to the island while in region 1. Ideally these two values should be equal at all times. This helps to show how the trained machine has greater difficulty locating the island when the observer is further from the island.

aforementioned controls for either of the two boundaries at random and reestimate at the next time epoch. Following these rules and re-evaluating at regular intervals will eventually get you to visible sight of the island, where human navigation or other forms of navigation (e.g., vision-aided) could take over. This form of navigation might mimic to a degree, how the Marshallese sailors would sense the interaction between the swell and reflected wave and follow the interaction to the island.

B. *Localization*

For each region two regression machines were trained. One machine was responsible for finding the distance to the island in the x direction and the other machine was responsible for finding the distance in the y direction. Similarly to the classification case, a parametric study was preformed to see which kernel was best able to determine the island's location, because there were multiple machines being trained, each one was given its own parametric study. For all studies, it was found that a Matern $\frac{5}{2}$ Gaussian Process Regression (Matern-GPR) had the lowest error for all regions and directions with an average RMSE of 40 nodes.

The RMSE for each of the trained machines are shown in Fig. 10. The RMSE for each of the machines vary widely and are larger than desired with and average RMSE of 40 nodes. An error greater than ten implies we would not be able to navigate to the island within sight range. Regions 1 and 3 both have a smaller error predicting the x direction while regions 2 and 4 had a smaller error in the y direction.

For further examination, a new set of regressors were trained with the assumption that the swell wave could be parsed/sensed

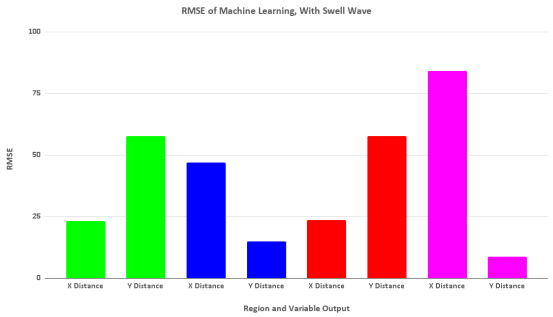

Fig. 10. Localization via learned regressor: Each bar shows the average error of a trained predictor when estimating the location of the island with respect to an observer in a known region. The green bars are for region 1, blue in region 2, red in region 3 and magenta in region 4.

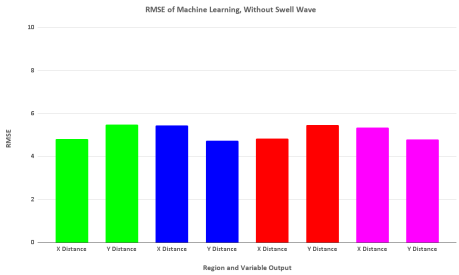

Fig. 11. Localization via learned regressor after swell subtraction: Each bar shows the average error in predicting the location of the island (relative to an observer) when the swell wave was removed. The green bars are for region 1, blue in region 2, red in region 3 and magenta in region 4.

and removed from the overall wave signal. This was done to examine if the presence of the swell wave increased the RMSE in the trained machines. Figure 11 shows that when the swell wave is removed, the error drops significantly to an average RMSE of 5 nodes. Further exploration of the data is required here to understand why the error reduction was so dramatic without the swell, and if it is practical to be able to remove the swell component when performing this in situ with humans or robots at sea.

V. Conclusion and Future Work

Regressors trained via supervised learning show that it is possible to determine the location of an island assuming that the reflected wave can be differentiated from the swell wave. Knowing the location of the island might be used in tandem with dead reckoning to globally localize your location.

We have designed a scale model boat (see Fig. 12), and integrated a small CPU and off-the-shelf sensors (compass, IMU, etc.) to begin in situ testing. The scaling for the boat was done using Buckingham's Pi Theorem, keeping a geometric similarity between oceanic conditions in the Marshall islands and values achievable with a wave flume. The geometric similarity assures that the water wave motion in the model simulates a larger device in the ocean. Initial experiments will

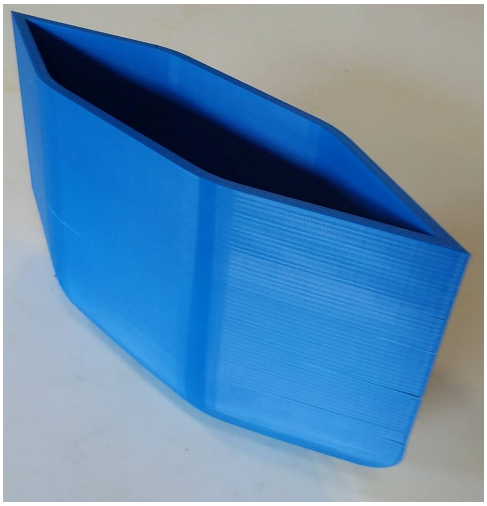

Fig. 12. Our 3D printed model of boat for collection of wave information.

use the scale-model boat in a wave flume. The goal of these experiments will be to see if a single IMU will be able to sense the wave parameters seen in the model analysis in a way that would allow the machine learning methods to accurately determine the direction of land.

Acknowledgments

This work was supported in part by the National Science Foundation via NSF MRI 1531322, IIS-1453652, the US Office of Naval Research Award N00014161263, and by the U.S. Department of Homeland Security under Grant Award Number 2017-ST-062000002.

References

[1] M. Ascher, "Models and Maps from the Marshall Islands: A Case in Ethnomathematics," *Historia Mathematica*, vol. 22, pp. 347–370, Nov. 1995.

[2] K. Akerblom, *Astronomy and Navigation in Polynesia and Micronesia*. Stockholm: Ethnographical Museum, 1968.

[3] M. George, "Polynesian Navigation and Te Lapa—The Flashing," *Time and Mind*, vol. 5, no. 2, pp. 135–173, 2013.

[4] M. Ford, M. A. Merrifield, and J. M. Becker, "Inundation of a low-lying urban atoll island: Majuro, Marshall Islands," *Natural Hazards*, vol. 91, pp. 1273–1297, Apr. 2018.

[5] J. Genz, "Complementarity of Cognitive and Experiential Ways of Knowing the Ocean in Marshallese Navigation," *Ethos*, vol. 42, pp. 332–351, Oct. 2014.

[6] C. C. Pyrek and R. Feinberg, "The Vaeakau-Taumako Wind Compass as Part of a Navigational Toolkit," *Structure and Dynamics*, vol. 9, no. 1, pp. 41–69, 2016.

[7] H. Lyons, "The Sailing Charts of the Marshall Islanders," *The Geographical Journal*, vol. 72, pp. 325–327, Oct. 1928.

[8] W. Davenport, "Marshall islands navigational charts," *Imago Mundi*, vol. 15, pp. 19–26, Jan. 1960.

[9] T. Moran, "Introducing Micronesian stick charts as models of visual technical communication," in *IEEE International Professional Communication Conference*, (Limerick, Ireland), 2015.

[10] C. J. Davis, "Stick Charts of Micronesia," *Navigation*, vol. 11, no. 1, pp. 32–37, 1964.